R-curves of lead zirconate titanate (PZT)

Thomas Karastamatis[a], Doru C. Lupascu[b], Sergio L. dos Santos e Lucato[b],
Jürgen Rödel[b], Christopher S. Lynch[a],*

[a]*The G.W.W. School of Mechanical Engineering, The Georgia Institute of Technology, Atlanta, GA 30332-0405, USA*
[b]*Institute of Materials Science, Technical University of Darmstadt, Petersenstrasse 23, 64287 Darmstadt, Germany*

Abstract

R-curves were measured for ferroelectric ceramic lead zirconate titanate (PZT) using surface cracks in flexure (SCF) in a single composition of unpoled, ferroelastic PZT. The effects of several parameters on the *R*-curves were experimentally determined. These included grain size, indentation load, polishing away the residual stress zone associated with the Knoop indentation, and thermal depolarization after indentation. The larger grain size resulted in a higher plateau value of the *R*-curve, a result consistent with the larger amount of ferroelastic switching observed in the stress/strain curve. Increasing the indentation load from 10 to 50 N resulted in larger initial crack sizes. This had some effect on the early part of the *R*-curve, but did not much affect the plateau value. Polishing away the residual stress zone eliminated the residual stress contribution of the Knoop indentation to the stress intensity factor. This resulted in the most accurate measurement of the intrinsic toughness (0.4 MPa m$^{1/2}$). Thermal depolarization to remove any potential ferroelastic crack tip switching zone associated with the indentation had little or no effect on the measured *R*-curves.
© 2002 Published by Elsevier Science Ltd.

Keywords: Ferroelectric properties; Fracture; PZT; *R*-curves

1. Introduction

Most ferroelectric device failures are associated with brittle fracture. Fracture often originates at locations where there are field concentrations (mechanical or electrical), such as defects, inhomogeneities, cavities, or the ends of partial electrodes.[1] Understanding the fracture behavior and the underlying mechanisms should lead to improved reliability in design of actuators. The fracture behavior of lead zirconate titanate ceramics is complex and not yet fully understood. Important fracture parameters include the fracture toughness, *R*-curve behavior, and subcritical crack growth behavior, all of which are influenced by the polarization state and electric field levels. Many earlier works have addressed the fracture toughness of ferroelectric ceramics. Only recently have researchers begun to recognize the importance of *R*-curve behavior and subcritical crack growth to development of actuators with long term reliability. In materials that display *R*-curve behavior, the resistance to crack growth is a function of the amount a crack has grown. This is due to hysteretic deformation processes that occur in the high stress zone near the crack tip modifying the stress field in the wake of the crack.

Over the past four decades there have been many measurements of the fracture toughness of ferroelectric ceramics with many apparently conflicting results reported due to multiple parameters affecting the fracture toughness. These include composition (lead zirconate to lead titanate ratio dictates crystal structure), dopants (acceptor, donor, or mixed doping), grain size, polarization state, electrical boundary conditions (open vs. short circuit or applied electric field), orientation of crack relative to polarization, loading rate, and amount of crack growth.

Many test techniques have been used to characterize the fracture behavior of ferroelectric ceramics. The semi-qualitative Vicker's indentation technique has been used to show that fracture toughness is anisotropic in the polarized state, with lower toughness for a crack propagating perpendicular to the polarization direction.[2–5] The observed behavior has been attributed

to several phenomena including domain reorientation,[3,5] crack tip behavior,[6] and residual stress anisotropy,[2] and polarization induced anisotropy in the constitutive relations. The indentation technique is described as semi-quantitative because the polarization texture (state of polarization) induces elastic, piezoelectric, and dielectric anisotropy that are not accounted for in the experimentally calibrated equations for calculation of fracture toughness.[7] Knowledge gained from indentation results was improved upon by compact tension work performed by Park and Sun[8] and Lucato et al.[9] In the work of Park and Sun, it was shown that electric field in the direction of polarization reduces the toughness and opposite the electric field direction enhances toughness. It is not clear from the study whether the results apply generally to rhombohedral, tetragonal, morphotropic boundary, soft, and hard compositions or only to the specific composition used in the study.

More recently, researchers have begun measuring *R*-curves in ferroelectric ceramics. Meschke et al.[10] measured *R*-curves for BaTiO$_3$ using compact tension (CT) specimens, and found that the toughness increased from initial values of 0.5–0.7 MPa m$^{1/2}$ to peak values of 0.7–1.2 MPa m$^{1/2}$, depending on grain size. Munz et al.[11] and Lucato et al.[9] performed similar tests on PZT and found that their material displayed similar *R*-curve behavior. Lucato et al.[9] reported *R*-curves as a function of initial polarization direction.

This work focuses on application of the surface crack in flexure technique (SCF). The SCF technique offers a means to characterize cracks on the size scale of the microstructure. Such cracks are more representative of flaws that lead to failures in real materials than through cracks in CT specimens. Chen et al.[12] used this technique to measure *R*-curves for two compositions of lead lanthanum zirconate titanate (PLZT). The 8/65/35 hot pressed composition exhibited ferroelastic behavior and the 9.5/65/35 hot pressed composition exhibited quadratic electrostrictive linear elastic behavior. Both compositions were transparent. The technique used involved inducing a semi-elliptical surface crack by Knoop indentation, and then polishing away the residual stress zone formed by the indent. The technique was similar to that used by Stech and Rödel[13] to measure *R*-curves in alumina and alumina/aluminum composites. Chen et al.[12] were able to measure the aspect ratio during crack growth because the specimens were transparent, but they used an analysis of their data that assumed linear stress strain behavior when they applied the equations developed by Newman and Raju.[14] The ferroelastic behavior violated the linear elastic assumption. Chen et al.[12] were able to measure the nonlinear stress/strain behavior from the four-point bend specimens using an approach discussed by Nadai[15] and first applied to PZT by Fett et al.[16] This approach allowed them to

accurately calculate the stresses on the tensile and compressive surfaces of the beam. The problem still existed, however, that the equations of Newman and Raju[14] assume a linear stress distribution through the thickness of the beam.

This work reports the results of an experimental study performed using the SCF technique to determine the effects of grain size, indentation load, polishing away the residual stress zone created by the indent, and thermal depoling on the measured *R*-curve behavior. The analysis approach is modified to correct for the nonlinear stress distribution through the thickness of the beam.

2. Experimental setup and procedure

2.1. Material description and specimen preparation

A commercial composition of PZT was used in this study, TRS600 (TRS Ceramics, State College, PA USA). The composition lies at the morphotropic boundary and the material is donor doped. At room temperature this composition is below the Curie temperature and is both ferroelectric and ferroelastic. The material is translucent but not transparent. The specimens came from two different batches with average grain sizes of 1.4 and 5 μm, respectively.

Specimens were cut into bars $3 \times 4 \times 25$ mm^3. The specimens were then prepared as described by Stech and Rödel.[13] The bars were polished to a 1 μm finish on the 4×25 mm^2 surfaces. All specimens were unpoled.

2.2. Experimental arrangement

A four-point bend device with inner and outer spans of 10 and 20 mm was used. The load was applied using a piezoelectric stack actuator and monitored by a load cell. The fixture was designed to fit into either an optical or scanning electron microscope. Specimens were viewed on the tensile side so that growth of flaws could be monitored from the surface.

The crack length and the applied load were recorded to obtain *R*-curves. During the experiments, the crack moved continuously. The crack velocity was maintained below 1 μm/s. During the crack growth, the load was decreased to prevent the crack from accelerating. The crack length and load data were used to calculate the applied stress intensity factor, K_I.

2.3. Experimental procedure

An initial set of experiments was performed to determine the stress/strain behavior of the material. Strain gages were applied to the tensile and compressive surfaces of polished bend specimens without preexisting

surface cracks. The specimens were placed in the four-point bend device. Strain and applied load data were recorded. This data was analyzed to determine the stress distribution in the beams.

Next, a set of experiments was performed to collect *R*-curve data for various values of the four parameters. A Knoop indentation was made in the center of the large face of the specimens using either a 10 or 50 N load. The crack observed on the surface was perpendicular to the long edges of the beam. This resulted in semi-elliptical surface cracks for both grain sizes and indentation loads. Strain gages were not placed on the SCF specimens. The stress/strain data collected in the first set of tests was used in the data analysis.

The test matrix is shown in Table 1. Several parameters were experimentally varied to determine the effects of grain size, indentation load (i.e. initial flaw size), polishing away the residual stress zone caused by the indentation, and thermal depoling (TDP) on the measured *R*-curve behavior. The measured *R*-curves for each set of test parameters are compared with a reference *R*-curve.

The reference *R*-curve was measured from a fine grained specimen, indented with a 10 N Knoop, and then polished to remove the damage/residual stress zone created by the indentation. The specimen was not thermally depoled. After polishing, a semi-elliptical surface flaw remained. Parameter differences between the reference *R*-curve and each of configurations are summarized in Table 1. In configuration 1 the indentation load was increased to 50 N. In configuration 2 the grain size was increased to 5 μm. In configuration 3 the residual stress damage zone was not polished away after the indentation was made. In configuration 4 the material was thermally depoled. The specimens were heated above the Curie temperature for 1 h at 250 °C to eliminate any process zone at the crack front caused by the indentation. The Curie temperature provided by the manufacturer is $T_c = 190$ °C. The specimens were then polished to remove the damage zone created by the indentation. The process of TDP then polish was selected because the reverse order, polish then TDP, seemed to produce some crack healing and obscured the initial crack growth data. In configuration 5, the indentation

load was 50 N and the damage zone was not polished away.

The aspect ratio of the semi-elliptical cracks was measured as a function of crack growth by slowly growing cracks to different lengths and then rapidly breaking the specimens. The aspect ratios were determined from the fracture surface. The transition from stable to unstable crack growth left a clear marking. Rate dependence of the fracture toughness led to instability when the rapid load was applied. The fracture surfaces were viewed to measure the aspect ratio of the crack before it went unstable. To measure the aspect ratio, a fiber optic light was directed parallel to the fracture surface and the surface viewed in an optical microscope.

2.4. Experimental results and data analysis

The stress/strain behavior was measured in the first set of experiments using strain gages using the technique proposed by Fett et al.[16] The analysis of the strain gage and load data to obtain stress/strain curves for a nonlinear material with hysteresis cannot be applied during unloading. Eqs. (1) and (2) give the stress on the compressive and tensile surfaces, respectively.

$$\sigma_1 = \frac{2M(\varepsilon_2 - \varepsilon_1)}{b\varepsilon_1 h^2} - \frac{\partial M}{\partial \rho}\frac{1}{bh\varepsilon_1} \tag{1}$$

$$\sigma_2 = \frac{2M(\varepsilon_2 - \varepsilon_1)}{b\varepsilon_2 h^2} - \frac{\partial M}{\partial \rho}\frac{1}{bh\varepsilon_2} \tag{2}$$

where M is the applied bending moment, b is the width of the beam and h is the height, ε_2 and ε_1 are the strain of the tensile and compressive surfaces respectively, and ρ is the radius of curvature.

The strains are known from the strain gages, the applied moment is known from the applied loads and loading geometry and the radius of curvature is given by Eq. (3).

$$\rho = \frac{h}{\varepsilon_2 - \varepsilon_1} \tag{3}$$

The moment and radius of curvature are measured as the beam is loaded. The moment is plotted against $1/\rho$. The resulting plot is curve fit using a third order polynomial. The polynomial is differentiated with respect to the radius of curvature to determine an equation for the partial derivative of the moment with respect to the radius of curvature. This is used with Eqs. (1) and (2) to obtain the stress/strain curves. The results are shown in Fig. 1. Loading of the ferroelastic material results in nonlinear behavior. There is an asymmetry between the tensile and compressive response. The coarse grain specimen displays more ferroelastic switching than the fine grain specimen. This is evident in the additional inelastic

Table 1
The test matrix of the parameters that were varied in the SCF tests

Configuration	Indentation load (N)	Grain size	Damage zone polished away	Thermally depoled (TDP)
Reference	10	Fine	Yes	No
1	50	Fine	Yes	No
2	10	Coarse	Yes	No
3	10	Fine	No	No
4	10	Fine	Yes	Yes
5	50	Fine	No	No

strain seen for the coarse grain material in Fig. 1. Unload curves are not shown because the flexural technique for measuring stress/strain curves is not valid for unloading when there is hysteresis present.

The stress-distribution through the thickness of the bend specimens was determined from the stress/strain data, the specimen height, and the applied moment. This is shown in Fig. 2. The stress distribution changes as the beam is loaded. The distribution shown in Fig. 2 corresponds to the reference R-curve when the maximum stress was applied to the beam. The Newman and Raju equations used for determination of fracture toughness from crack length and load data account for the stress gradient in the beam by assuming a linear stress distribution (linear elastic material response). To correct for this, the stress gradient assumed in the analysis can be matched to the stress gradient in the region of interest (depth of the crack) by increasing the beam thickness in the calculations. The thickness of the beam used in the Newman and Raju analysis was 2.2. times the actual thickness of the beam. The effect of changing the thickness in the analysis to match the stress gradient is illustrated in Fig. 2.
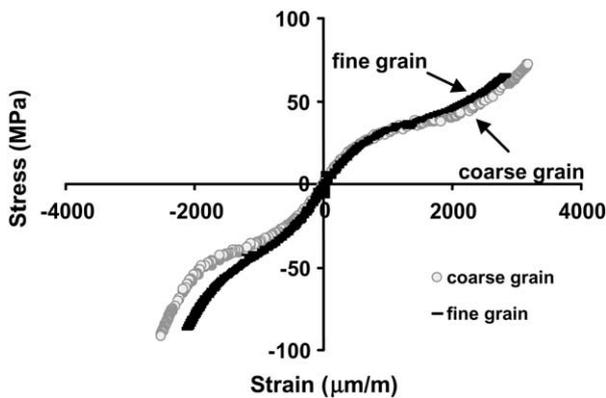

Fig. 1. The bending stress calculated from strain gage and applied load data is shown. There was not a significant difference in the stress/strain behavior between the two grain sizes.
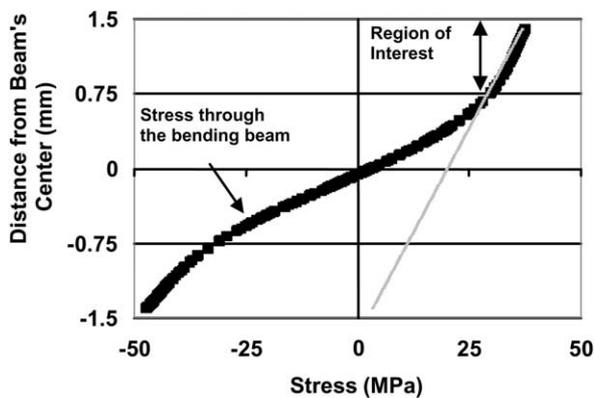

Fig. 2. The stress distribution through the thickness of the beam is shown at the peak load. The non-linearity must be accounted for in the analysis of the R-curve data.

Knowledge of the crack aspect ratio is necessary to determine K_I from the crack length vs. load data. The results of crack aspect ratio measurements at different crack lengths are shown in Fig. 3. A typical fracture surface from which the aspect could be measured is shown in Fig. 4. The average value of the measurements was used in the analysis.

The measured R-curves were obtained from load vs. crack growth data. The load had to be reduced as the crack grew to maintain constant propagation velocity. The load as a function of crack length required to maintain a constant crack velocity is shown in Fig. 5. Fig. 5a shows the results for different grain sizes and indentation loads. Fig. 5b shows the results for polishing and thermal depoling. After a certain amount of crack growth, the load drop becomes significant. This introduces some error in the calculated plateau of the R-curves since the reduction of load for an elastic-plastic bar results in a complex state of macroscopic residual stress. The worst cases are the reference configuration
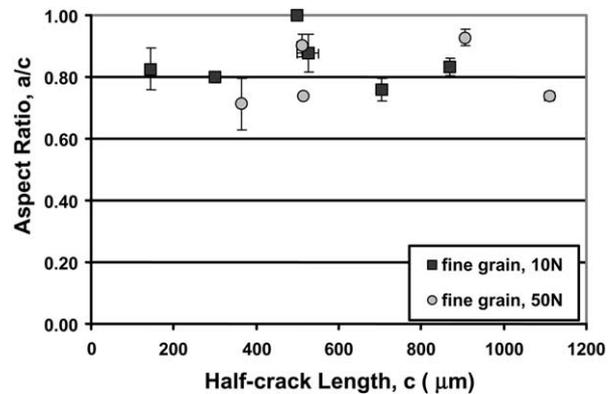

Fig. 3. The aspect ratios measured from the fracture surface are shown.

Fig. 4. A fracture surface from which the aspect ratio was measured. The semi-ellipse is visible because the sub-critical crack growth is transgranular, while the super-critical crack growth is intergranular. When light is parallel to the fracture surface, the semi-ellipse becomes visible.

and configuration 4 where the load drop is in excess of 15% from the peak load.

The fracture toughness was calculated during crack growth using Eq. (4).

$$K_I = H\left(\frac{a}{t}, \frac{a}{c}, \Phi\right)\sigma_b \sqrt{\frac{\pi a}{Q\left(\frac{a}{c}\right)}} F\left(\frac{a}{t}, \frac{a}{c}, \frac{c}{b}, \Phi\right) \qquad (4)$$

(for $0 < a/c \leqslant 1$, $0 < 0.8$, $c/b < 0.5$, $0 \leqslant \Phi \leqslant \pi$) where the expressions for H, Q, and F can be found in Newman and Raju.[14]

The results are shown in Fig. 6. Initial crack growth was in the linear-elastic region of the stress/strain curve. In this region the nominal thickness, t, could be used. Since the modification of the thickness introduces a very small error for small amounts of crack growth and the load rapidly rises to its peak value, the modified thickness was used for the entire calculation of the R-curves. For the cracks created by the 10 N indentation, $t' = 2.2t$ was used, while for the larger initial flaw size created by the 50 N indentation, a modified thickness $t' = 1.5t$ was used. The modified thickness was taken from the stress-distribution through the beam at the point of maximum applied stress and was only valid for a crack depth $a < 700$ μm.

3. Results

The measured R-curves are shown in Fig. 6. The results of the reference R-curve measurement (fine grain specimen, 10 N indent, damage zone from indent polished, no TDP) are an initial toughness of $K_{Ii} = 0.4$ MPa m$^{1/2}$ and a maximum toughness $K_{Im} = 0.94$ MPa m$^{1/2}$ measured at the surface of the crack ($\phi = 0°$). Only values of fracture toughness at the intersection of the crack with the specimen surface were calculated because there is significantly more error associated with calculating the fracture toughness for the bottom of the crack. At the bottom of the crack the decrease in load and the non-linear stress distribution induce a much larger error. The intrinsic toughness is taken as the point where the R-curve changes slope from vertical to a negative curvature.

Configuration 1, for the 50 N indent with the residual stress zone polished out, displays a comparable intrinsic toughness, $K_{Ii} = 0.4$ MPa m$^{1/2}$ and a slightly lower plateau value than the reference curve. This may be experimental error associated with the crack length
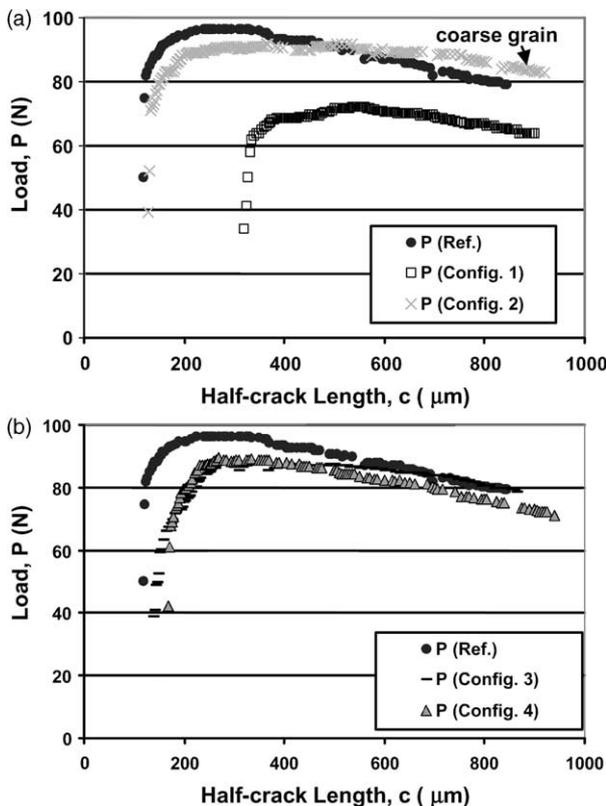

Fig 5. Applied load vs. half-crack length is shown. (a) The data are shown for different grain sizes and indentation loads (i.e. initial flaw size). (b) The data are shown for different specimen preparation conditions (i.e. polishing and thermal depoling).
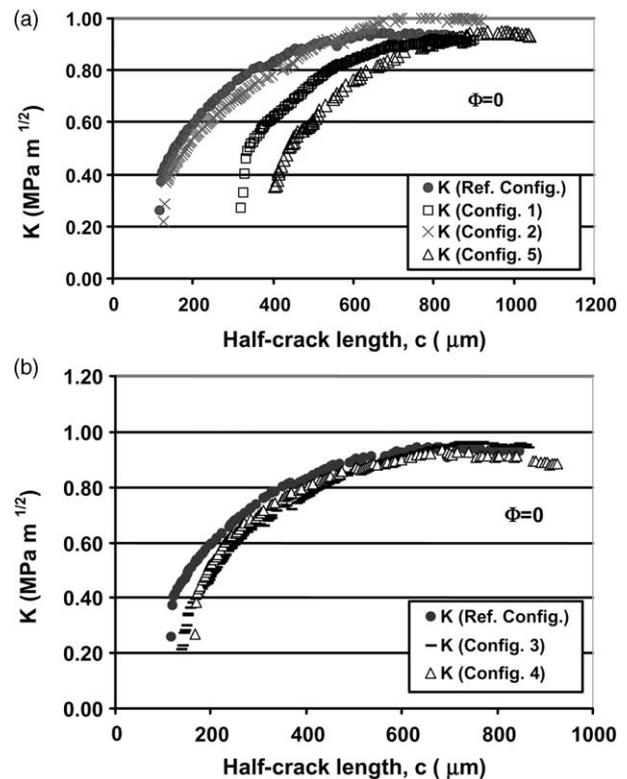

Fig 6. (a) R-curves in TRS600 coarse and fine grain PZT are shown. There is not a significant difference between the curves from different grain sizes. The larger initial flaw resulted in a lower plateau value. (b) R-curves in TRS600 fine grain PZT are shown. Not polishing away the damage/residual stress zone created by the indentation before testing did not have a significant effect on the R-curve behavior. Thermally depoling (TDP) before polishing away the damage zone did not have an effect on the R-curve behavior.

measurement. In the test technique, only one crack tip can be monitored under the microscope.

Configuration 2, the coarse grain material, had the same or slightly lower intrinsic toughness, but displayed a higher R-curve plateau. The peak toughness was $K_{Im} = 1$ MPa m$^{1/2}$. The higher plateau is attributed to a larger amount of ferroelectric switching induced toughening. The coarse grained material has the same critical switching stress but more inelastic strain (see Fig. 1). This results in more energy dissipation in the domain switching crack tip zone.

The results for configuration 3, not polishing away the damage/residual stress zone created by a 10 N Knoop indentation are $K_{Im} = 0.95$ MPa m$^{1/2}$. As the crack grew, the effect of the initial indentation residual stress zone had less effect on the R-curve behavior. The plateau value was the same as for the specimen with the damage zone polished away.

The results of configuration 4, TDP, are $K_{Im} = 0.93$ MPa m$^{1/2}$. TDP did not have a significant effect on the R-curve behavior. It is possible that TDP would have an effect on the measured intrinsic toughness, but to determine this would require performing the experiments at a higher magnification, such as in an SEM.

4. Discussion

The results of this study give insight into the fracture process. An atomically sharp crack front is a characteristic of brittle fracture. The mechanism of crack propagation is associated with the crack tip. The crack propagates when two planes of atoms are pulled apart, creating new surface. In ideal brittle fracture, the work to separate these planes of atoms is equivalent to the surface energy of the surfaces created. This work per unit crack advance is the intrinsic energy release rate and is associated with the intrinsic toughness through the Irwin relations. Identification of the intrinsic toughness of PZT is complicated by several factors. The material displays subcritical crack growth, a strong indication that one or more environmental species (water probably has the largest effect) contribute to a reduction of the surface energy. In the poled material, the constitutive behavior of PZT displays electro-mechanical coupling, and it is possible that the stretching of atomic bonds by an applied electric field contributes directly to the fracture process. Unlike mechanical forces, electric field penetrates a crack and is concentrated within. Fracto emission is known to occur when poled ferroelectric ceramics fracture. This includes phenomena such as triboluminescence and electron emission. Any electrical charge could form a charged surface layer that would reduce the electrical energy within the crack and could alter the surface energy. Such issues are not yet well

understood. In this work the focus was on unpoled specimens.

In the unpoled material, the fracture process is governed by the stress field very near the crack tip. In a linear elastic material this can be computed from the asymptotic solutions of the mode I loading together with specimen and load geometry. Since the K-fields are linear elastic, they can be combined using superposition. The applied K-field for the semi-elliptical crack with center point loads and remote tensile loading is given by

$$K_a = \psi\sigma\sqrt{\pi c} + 2\alpha P/(\pi c)^{3/2} \qquad (5)$$

where α is a constant, ψ contains corrections for stress gradient, aspect ratio, and geometry as discussed earlier, and c is the half crack length measured from the surface. When the indentation damage zone has been polished out, the point loads P go to zero and the second term drops out.

The applied remote tensile bending stress contributes to the crack opening an amount

$$2V = \chi\sigma c \qquad (6)$$

where $2V$ is the crack opening at the origin (center at surface) and the factor χ accounts for elastic moduli and crack geometry.

When the residual stress of the indentation is present, the residual wedge force of the indentation is sourced by a very small volume of damaged material within the crack. The wedge force P decreases as the bending stress is increased. If the wedge force, P, goes to zero during crack propagation i.e. the crack opening induced by the bending stress fully relieves P prior to crack growth, then the R-curve plateau will not be affected by the residual stress of the indentation.

A comparison of the initial crack propagation portion of the R-curves for the polished and unpolished specimens indicates that the residual wedge force is still contributing to K_a at the onset of crack propagation in the unpolished specimen. As the crack grows, this wedge force drops to zero due to both the increased crack opening reducing the wedge force and the reduction of stress intensity factor associated with the wedge force as the crack lengths increase. After about 75 microns of growth, the two R-curves converge.

The onset of crack growth for the specimens with the residual stress polished away is the most accurate measurement of the intrinsic toughness that was made. The measured intrinsic toughness (0.4 MP$\sqrt{}$m) has an error associated with effects of subcritical crack growth. In the experiments, the crack growth rate was maintained at around 1 micron per second. At present, V–K curves have been run in the laboratory environment. At 1 micron per second, the stress intensity factor is less than the maximum value measured at 1 cm per second.

This suggests that the intrinsic toughness of the material in vacuum would be higher.

The rising portion of the *R*-curve is the result of ferroelastic domain reorientation. The stress strain curve has an initial elastic response, an inelastic regime in which the tangent modulus drops, and inflection point where the tangent modulus begins to increase, and a second elastic regime at higher load. When this stress/strain behavior interacts with the *K*-field it gives rise to a domain reorientation zone that forms an annulus about the crack tip. Inelastic shear deformation is taking place within the major and minor radii of the annulus. Outside of the major radius the behavior is elastic and inside of the mirror radius the behaviour is also elastic. The far field is thus a *K*-field and the near field is a *K*-field of lower intensity. As the crack grows, the inelastically deformed material moves into the wake of the crack. The inelastic zone has the effect of reducing the crack opening. This reduces the stress at the crack tip. A larger applied stress intensity factor is therefore required to obtain the next increment of crack growth. This process reaches steady state as the crack grows.

The stress intensity in the presence of shielding can be expressed as

$$K_{\text{tip}} = K_a + K_\mu(\Delta c) \tag{7}$$

where K_{tip} drives the crack tip decohesion of atomic bonds, K_a is calculated from the applied load, and K_μ is a negative stress intensity factor that arises from the presence of the inelastic deformation. If K_{tip} is the intrinsic toughness (0.4 MPa$\sqrt{}$m) and K_a is the peak applied stress intensity (0.9–1.0 MPa$\sqrt{}$m), then the inelastic strain contributes a shielding at large delta C of (0.5–0.6 MPa$\sqrt{}$m).

Kinetics must again be mentioned. As with the measurement of the intrinsic toughness, the peak toughness measurement would be affected by subcritical crack growth. Although the applied stress factor intensity factor is higher after development of the *R*-curve, the tip stress intensity factor is believed to be the same. Subcritical crack growth is governed by the crack tip stress intensity factor and should therefore be independent of K_a as long as the crack growth rate is constant. For this reason, any effect on the intrinsic toughness measurement due to crack growth kinetics should also be present in the K_{tip} term used in determination of the shielding term.

5. Conclusions

R-curves were measured using the surface crack in flexing technique with four test parameters varied; grain size, initial flaw size, initial residual stress zone, and thermal depolarization. Polishing away the damage/residual stress zone created by a 10 N Knoop indentation does not significantly affect the *R*-curve, plateau value. Thermal depoling to relax the crack tip ferroelastic switching wake does not have a significant effect on either the *R*-curve initial or plateau value. The most significant effect was that a larger initial flaw size yields a lower *R*-curve plateau value. This is associated with the effect of large scale ferroelastic switching altering the stress field from linear elastic. This effect is smaller for larger flaws because the beam breaks at a lower maximum stress.

Acknowledgements

References

1. Winzer, S. R., Shankar, N. and Ritter, A. P., Designing cofired multilayer electrostrictive actuators for reliability. *J. Am. Ceram. Soc.*, 1989, **72**(12), 2246–2257.
2. Okazaki, K., Mechanical behavior of piezoelectric ceramics. *A. Ceram. Soc. Bull.*, 1984, **63**(9), 1150–1152.
3. Pisarenko, G. G., Chushko, V. M. and Kovalev, S. P., Anisotropy of fracture toughness of piezoelectric ceramics. *J. Am. Ceram. Soc.*, 1985, **68**(5), 259–265.
4. Mehta, K. and Virkar, A. V., Fracture mechanisms in ferroelectric–ferroelastic lead zirconate titanate (Zr:Ti = 0.54:0.46) ceramics. *J. Am. Ceram. Soc.*, 1990, **73**(3), 567–574.
5. Lynch, C. S., Fracture of ferroelectric and relaxor electroceramics: influence of electric field. *Acta Mater.*, 1998, **46**, 599–608.
6. Freiman, S., Fracture mechanisms in lead zirconate titanate ceramics. In *Fracture Mechanics*, ed. Evans *et al.* Plenum Press, New York, 1986.
7. Anstis, G. R., Chantikul, P., Lawn, B. R. and Marshall, D. B., A critical evaluation of indentation techniques for measuring fracture toughness: I, direct measurements. *J. Am. Ceram. Soc.*, 1981, **64**(9), 533–538.
8. Park, S. B. and Sun, C. T., Effect of electric field on fracture of piezoelectric ceramics. *Int. J. Fracture*, 1995, **70**, 203–216.
9. dos Santos e Lucato, S. L., Lupascu, D. C. and Roedel, J., Effect of poling direction on *R*-curve behavior in lead zirconate titanate. *J. Am. Ceram. Soc.*, 2000, **83**(2), 424–426.
10. Meschke, F., Kolleck, A. and Schneider, G. A., *R*-curve behavior of BiTiO3 due to stress-induced ferroelastic domain switching. *J. Eur. Ceram. Soc.*, 1997, **17**, 1143–1149.
11. Munz, D., Fett, T., Muller, S. and Thun, G. Deformation and strength behavior of a soft PZT ceramic, In *Proc. SPIE Vol. 3323, Smart Structures and Materials 1998: Mathematics and Control in Smart Structures*, ed. Vasundara V. Varadan, 1998 pp. 84–95.
12. Chen, W., Lupascu, D., Rödel, J. and Lynch, C. S., Short crack *R*-curves in ferroelectric and electrostrictive PLZT. *J. Am. Ceram. Soc.*, 2001, **84**(3), 593–597.

13. Stech, M. and Rödel, J., Method for measuring short-crack *R*-curves without calibration parameters: case study on alumina/aluminum composites. *J. Am. Ceram. Soc.*, 1996, **79**, 291–297.

14. Newman, J. C. and Raju, I. S., An empirical stress-intensity factor equation for the surface crack. *Engineering Fracture Mechanics*, 1981, **15**, 185–192.

15. Nadai, A., *Theory of Flow and Fracture of Solids,* Vol. 1. McGraw-Hill, New York, 1950 (Chapter 22).

16. Fett, T., Munz, D. and Thun, G., Nonsymmetric deformation behavior of lead zirconate titanate determined in bend tests. *J. Am. Ceram. Soc.*, 1998, **81**(1), 269–272.